Electronic Supplementary Material (ESI) for Journal of Materials Chemistry C.

Supporting Information

Three-dimensional self-similar super-repellent films for underwater display and switching wettability

Maolin Liu, Yuanfang Luo,* Demin Jia

School of Materials Science and Engineering, South China University of Technology, Guangzhou 510640, People's Republic of China

Corresponding Author

*E-mail: psyfluo@163.com

1. Fabrication, morphology and wettability analysis of the SSF

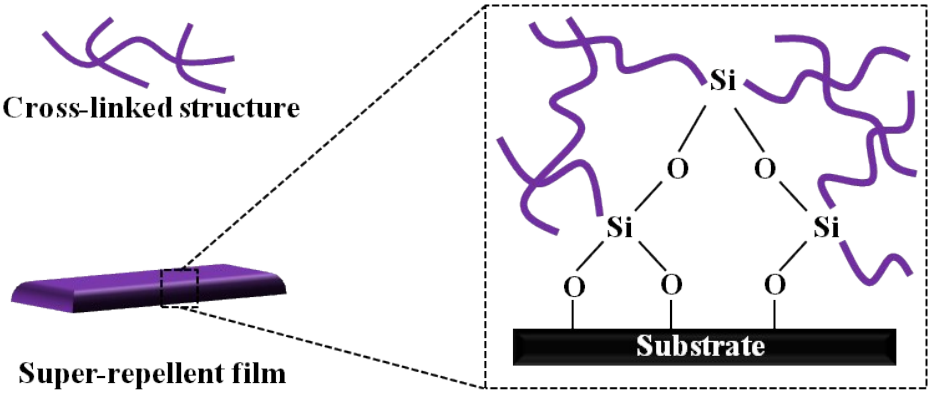

Fig. S1. Schematic illustration of the condensation reaction between glass substrate and reactants.

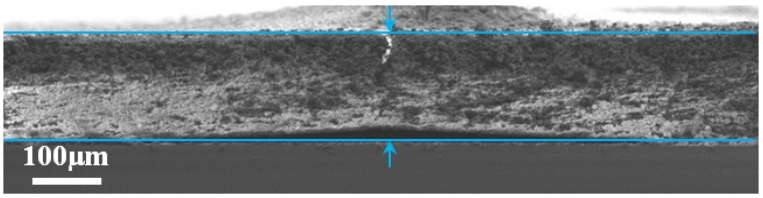

Fig. S2. Cross-sectional SEM image of the SSF.

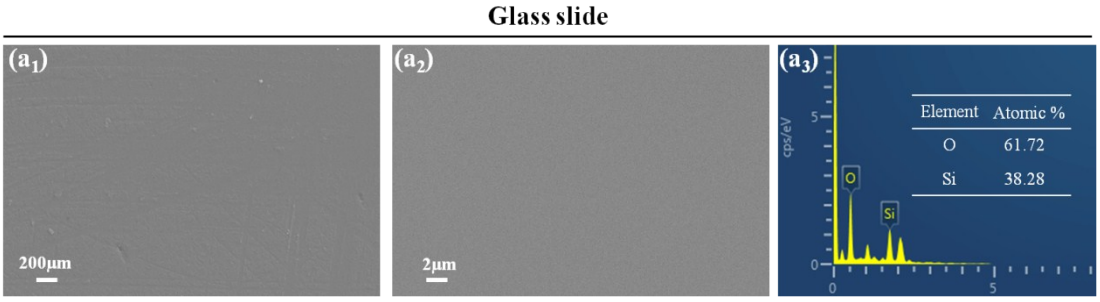

Fig. S3. (a_1, a_2) SEM images and (a_3) EDS spectrum of glass slide.

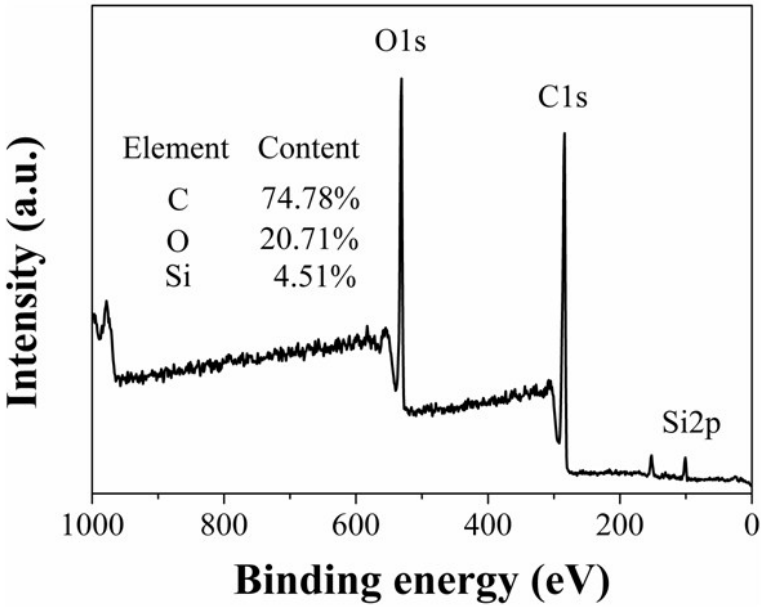

Fig. S4. XPS spectrum of the SSF.

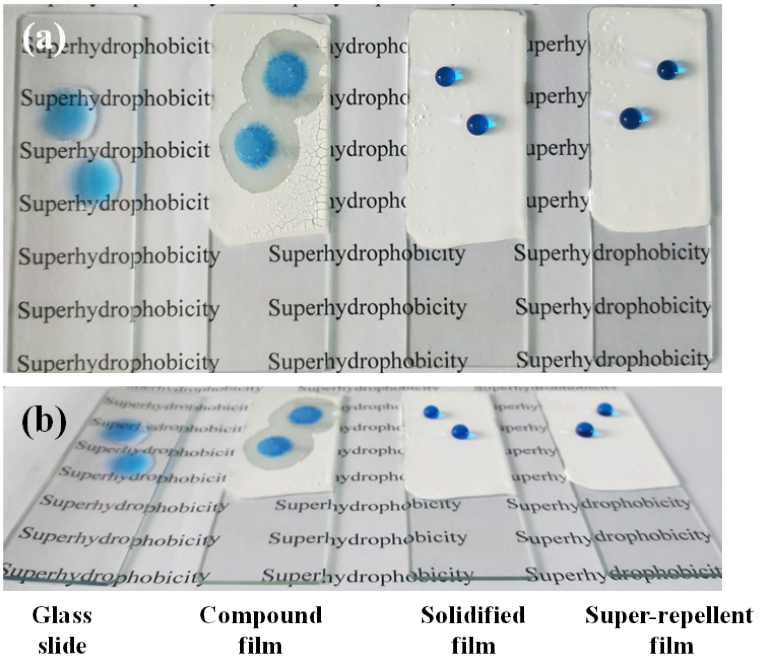

Fig. S5. Optical images of glass slide and different films.

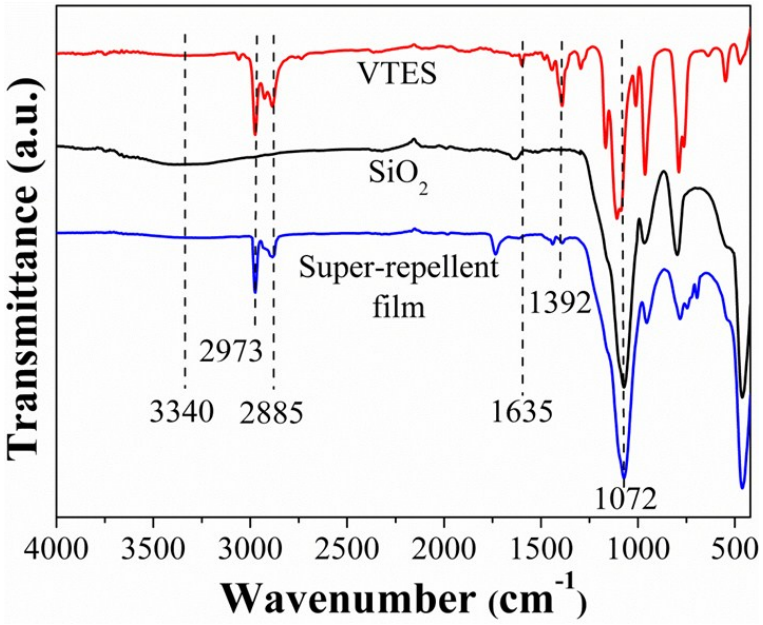

Fig. S6. ATR-FTIR spectra of different reactants and SSF.

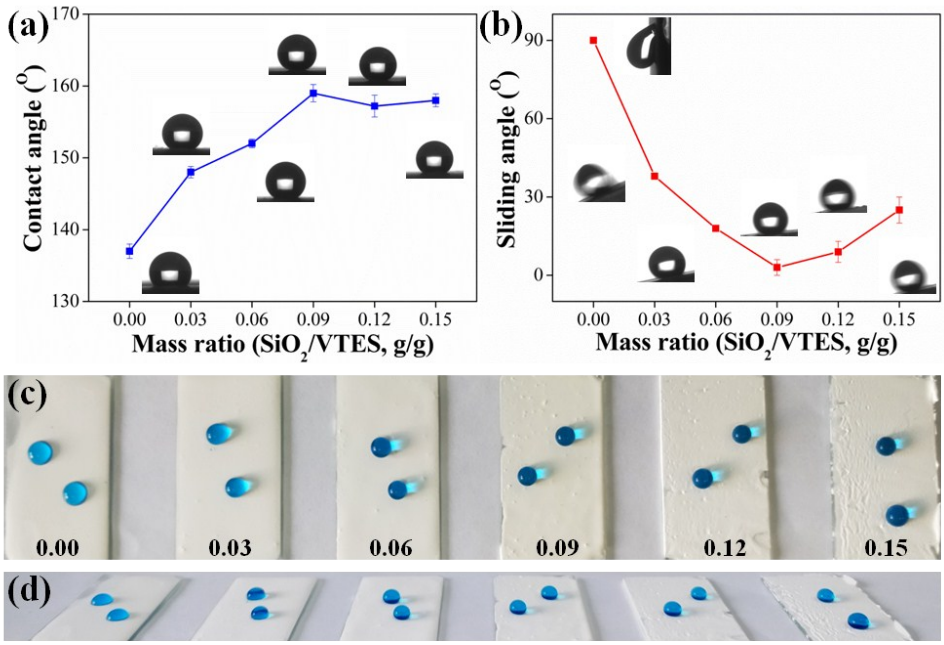

Fig. S7. (a) CAs and (b) SAs of the as-prepared films with different mass ratios (insets were the corresponding CAs and SAs). (c) Top and (d) side optical views of water droplets on the as-prepared films with different mass ratios.

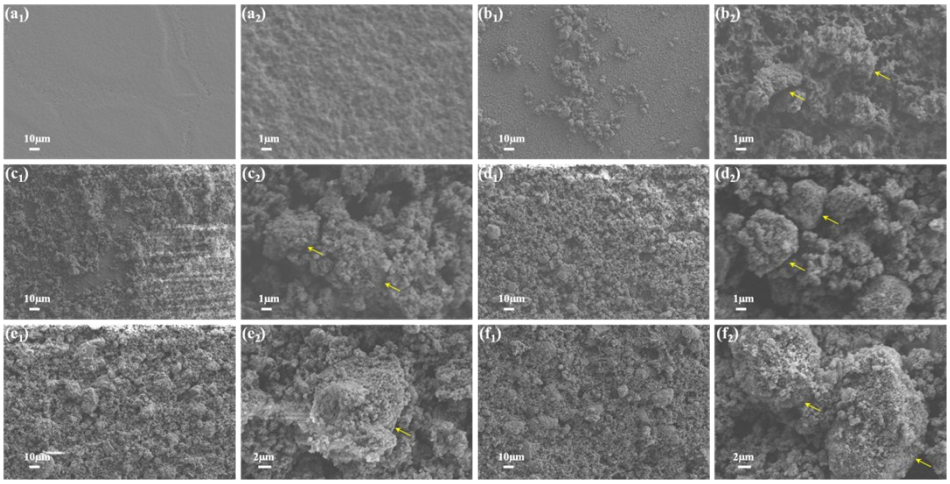

Fig. S8. SEM images of the as-prepared films with different mass ratios: (a_1, a_2) 0.00, (b_1, b_2) 0.03, (c_1, c_2) 0.06, (d_1, d_2) 0.09, (e_1, e_2) 0.12 and (f_1, f_2) 0.15.

2. Self-similar structure and continuous super-repellency of the SSF

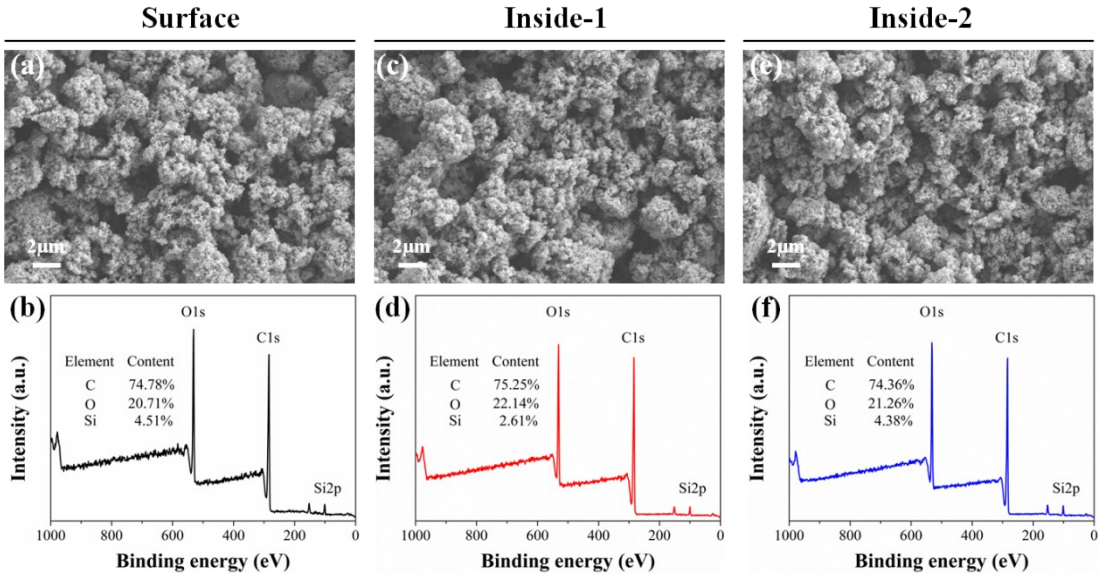

Fig. S9. (a, c, e) SEM images of the surface, inside-1 and inside-2 of the SSF, respectively. (b, d, f) Corresponding XPS spectra and element weight percentages of (a, c, e), respectively.

To confirm the three-dimensional self-similar structure throughout the thick film, the morphologies of surface and insides and the corresponding chemical compositions were characterized by SEM and XPS, respectively (Fig. S9). As shown in Fig. S9a, the micro-nano hierarchical structure constructed by SiO_2 was obviously observed, and the contents of C, O and Si were 74.78%, 20.71% and 4.51% (Fig. S9b), respectively, demonstrating the low-surface-energy surface. More importantly, measurement results in Fig. S9c-f show almost the same rough architecture and chemical properties as that of the surface of film, indicating the three-dimensional and self-similar super-repellency throughout the whole film. Thus, the combination of hierarchical rough structure formed by SiO_2 and crosslinked low-surface-energy structure supplied by polymerized vinyl monomers results in the three-dimensional self-similar structure, which benefits the super-hydrophobicity, and physical and chemical stability.

Video S1. Water flow bouncing on the SSF.

Table S1. CAs and SAs of surface and insides of different films

Mass ratio (SiO_2/VTES, g/g)	0		0.03		0.06		0.09		0.12		0.15	
	CA(°)	SA(°)	CA(°)	SA(°)	CA(°)	SA(°)	CA(°)	SA(°)	CA(°)	SA(°)	CA(°)	SA(°)
Surface	137±1	90±0	148±1	38±1	152±1	18±2	158±2	2±2	157±2	9±2	156±1	25±4
Inside-1	134±2	90±0	144±2	40±3	154±3	14±1	156±2	1±3	156±1	12±3	155±1	24±2
Inside-2	135±2	90±0	145±2	35±2	152±2	12±2	158±3	3±2	156±3	10±2	156±1	20±2

Table S1 tabulated the wettability of different films fabricated with different mass ratio of SiO_2 to VTES. As can be seen, the wettability of randomly exposed interiors (inside-1 and inside-2) of different films was almost the same as that of the corresponding surfaces. Undoubtedly, these phenomena resulted from the well-designed self-similar structure throughout the thick film, endowing the synthesized film with similar performance and continuous property visually as discussed previously.

3. Physical and chemical stability of the SSF

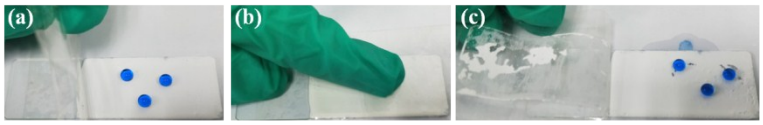

Fig. S10. Tape-peeling process on the SSF: (a) water droplets beaded on the intact SSF before tape-peeling test, (b) tape was tightly adhered to the SSF under pressure and (c) water droplets beaded on the damaged SSF after 30 cycles tape-peeling test.

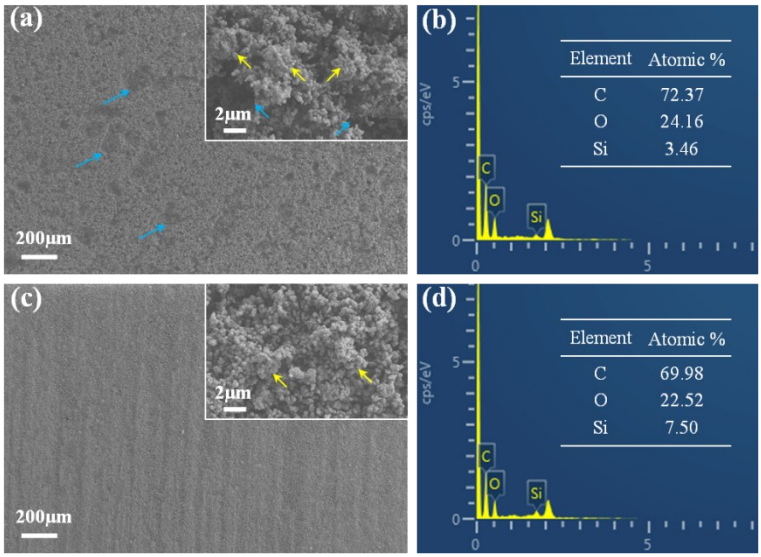

Fig. S11. (a) and (b) were the corresponding SEM images and EDS spectrum after tape-peeling cycles of 30, respectively. (c) and (d) were the corresponding SEM images and EDS spectrum after sandpaper abrasion cycles of 60, respectively.

Video S2. Knife scraping process and water repellency of the SSF.

Video S3. Self-cleaning behavior of the SSF after sandpaper abrasion cycles of 60.

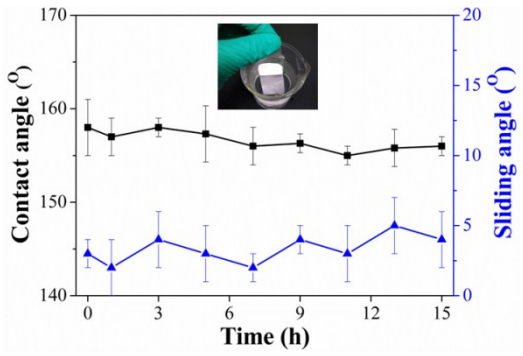

Fig. S12. CAs and SAs of the SSF after being exposed to ice water (inset was the experimental condition).

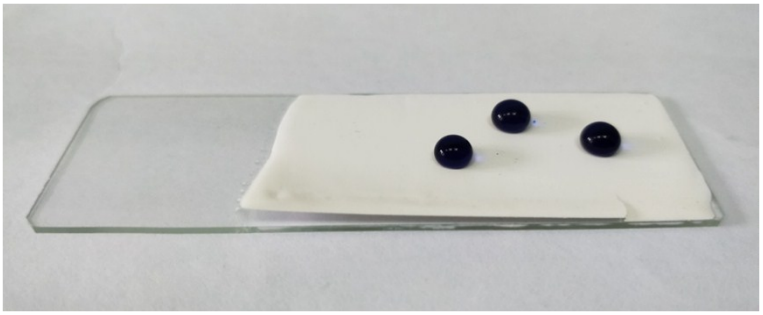

Fig. S13. Optical image of the SSF after being exposed outdoors for 3 months (inset was the CA of water droplet on the exposed SSF).

4. Pattern manipulation of the SSF for underwater display

Video S4. Underwater display of the patterned SSF.

5. Erasion healing of the SSF for switching wettability

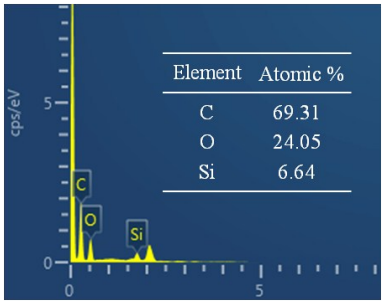

Fig. S14. EDS spectrum of the erasion healing SSF with 1 cycle.

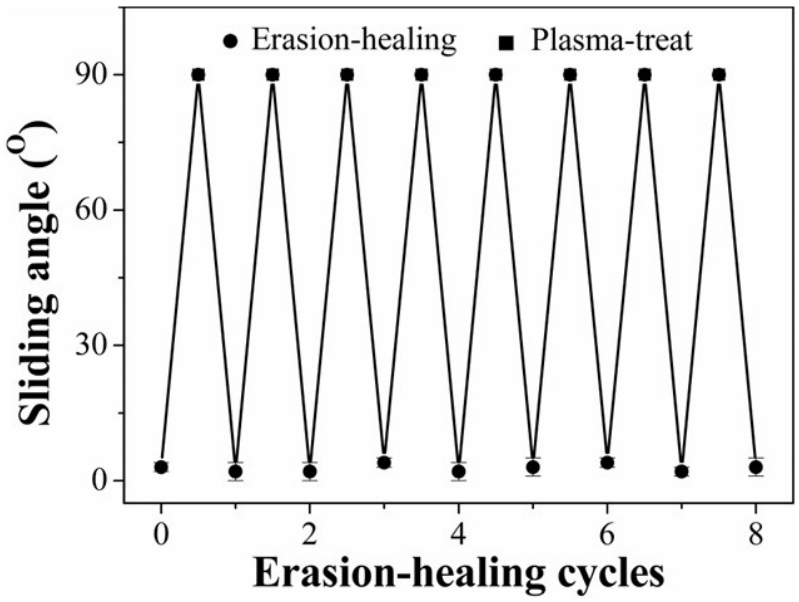

Fig. S15. SAs of the SSF with erasion healing cycles.

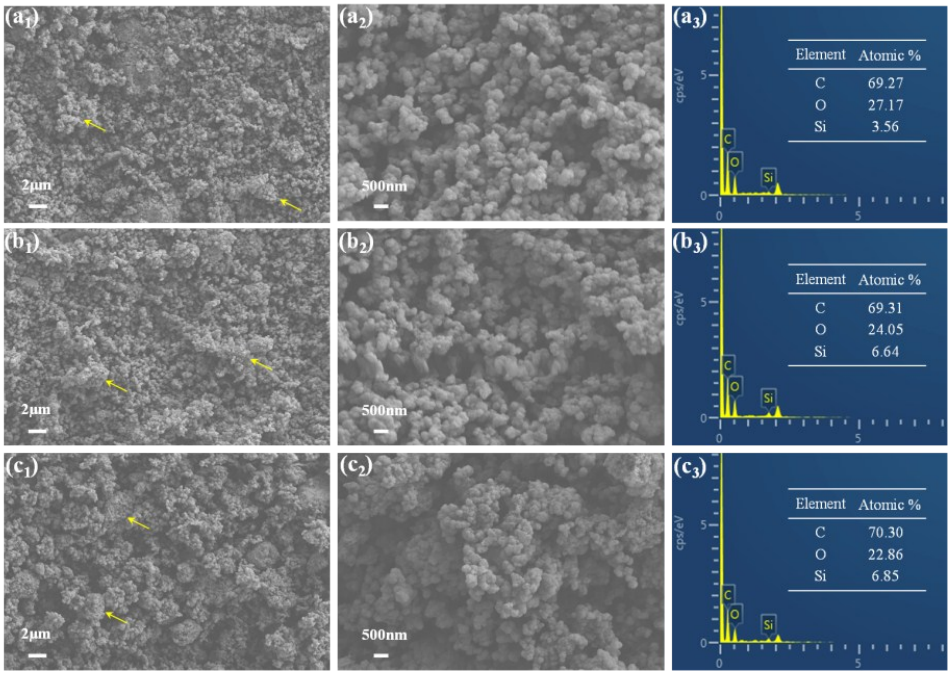

Fig. S16. SEM images and EDS spectra of the erasion healing SSFs: (a_1-a_3) 2 cycles, (b_1-b_3) 3 cycles and (c_1-c_3) 4 cycles.

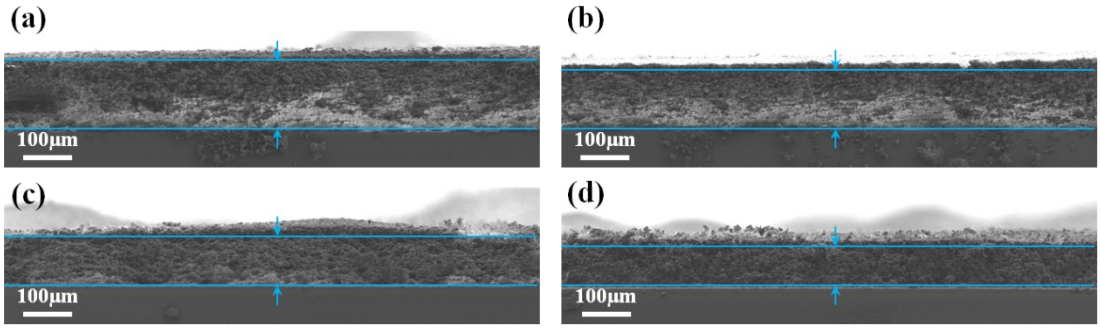

Fig. S17. Cross-sectional SEM images of the erasion healing SSFs: (a) 1 cycle, (b) 2 cycles, (c) 3 cycles and (d) 4 cycles.

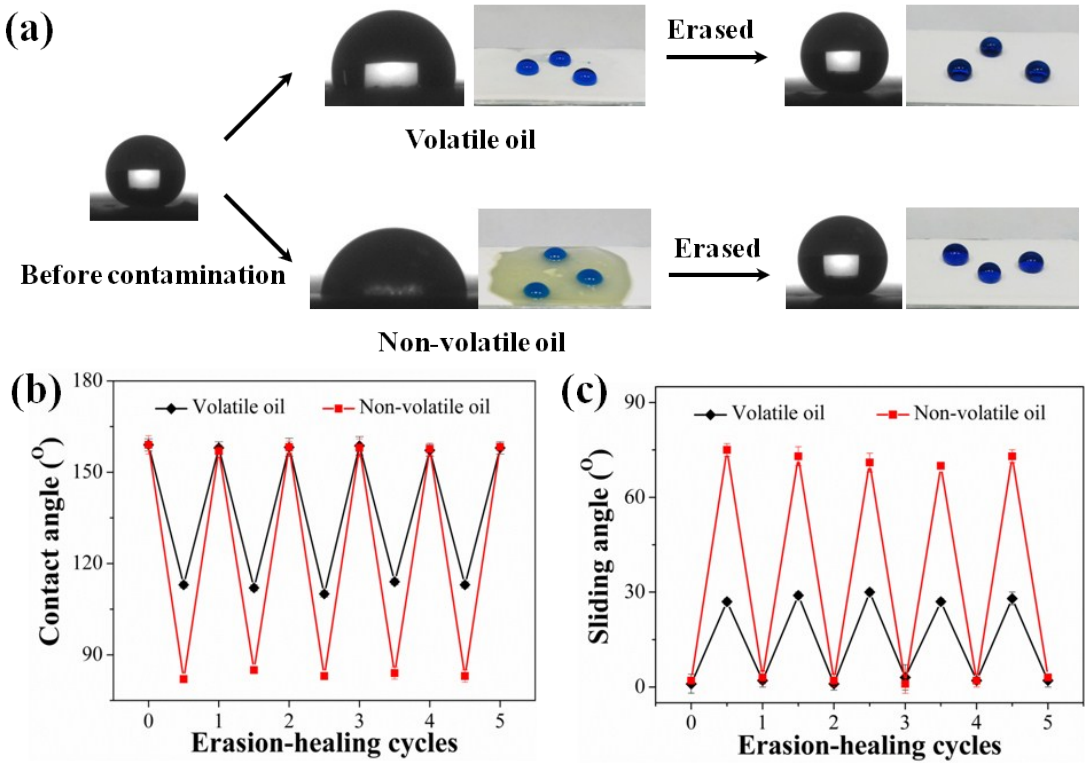

Fig. S18. (a) Erasion healing routes of the oil-contaminated SSFs. (b) CAs and (c) SAs of the SSFs with erasion healing cycles.

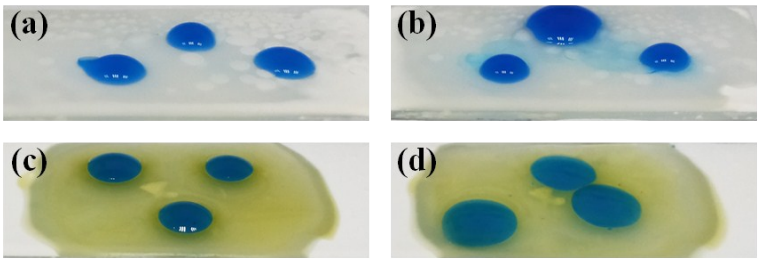

Fig. S19. Optical images of the oil-contaminated SSFs: (a) 1, 2-dichloromethane, (b) petroleum ether, (c) peanut oil and (d) engine oil.